International Journal of Advanced Engineering and Technology Research
ISSN: 3106-8677 (Print), ISSN: 3106-8685 (Online) | Vol. 2, No. 3, 2026

Smartphone Battery Life Prediction Based on Multi-Module Power Decomposition and Second-Order Thevenin Thermo-Electro Coupled Model

Jieming Yang [1, *], Xianzhi Zheng [2]

[1] Yunnan Agricultural University, Kunming, China
[2] Qujing Normal University, Qujing, China
[*] **Corresponding author**: (Email: 18387478815@163.com)

Abstract: This paper proposes a continuous-time forecasting method that integrates power consumption decomposition with battery state evolution for predicting smartphone battery life. The method unifies the modeling of power-consuming modules—such as the screen, CPU, network, GPS, and background activities—and combines them with a second-order Thevenin thermoelectric coupling model to describe the dynamic changes in SOC, voltage, polarization, and temperature. In the parameter estimation phase, least squares and weighted least squares estimation are introduced to improve the stability of the model fit. In the prediction phase, the remaining discharge time is calculated using the SOC decay relationship, and prediction reliability is evaluated through uncertainty propagation and sensitivity analysis. The results indicate that this model can reliably characterize battery discharge trends under various load conditions and demonstrates good transferability and practical value.

Keywords: Second-Order Thevenin Equivalent Circuit, Thermo-Electro Coupled Model, Least Squares Parameter Estimation.

1. Introduction

As the range of use cases for mobile devices continues to expand, battery power consumption exhibits distinct dynamic characteristics under the combined effects of high-brightness displays, multitasking, network transmission, location services, and concurrent background processes. Traditional battery life estimation methods often rely on a single average power consumption value or empirical curves, making it difficult to simultaneously reflect the relationship between external load changes and the evolution of the battery's internal state, which can lead to prediction errors in complex usage environments [1]. To improve the stability and interpretability of prediction results, this paper establishes a unified algorithmic model framework based on two levels: system power consumption sources and battery state responses. First, the device's total power consumption is decomposed into submodules such as the display, CPU, network, GPS, and background activities, forming an input-friendly and extensible power consumption expression. Second, a second-order Thevenin thermoelectric coupling model is introduced to incorporate SOC, voltage, polarization voltage, and temperature into a continuous-time state space, thereby enabling a coupled description of external power consumption and internal electrochemical responses [2]. Building on this foundation, a comprehensive remaining runtime prediction workflow is constructed by integrating parameter estimation, discharge time calculation, uncertainty propagation, and sensitivity analysis. Taking the prediction of smartphone battery discharge time as an example, this framework can characterize runtime trends under different initial charge levels and load conditions, providing a universally applicable modeling approach for mobile device energy consumption assessment and battery management.

2. Continuous-Time State-Space Modeling of Multi-Source Power Consumption and Battery Coupling

2.1. Multi-Module Power Decomposition Modeling Approach

During smartphone operation, battery power consumption is usually not driven by a single factor, but is the combined result of multiple functional modules, including the screen, processor, network connectivity, GPS, and background activities. Therefore, under a continuous-time modeling framework, total power consumption can be expressed as the sum of power consumption from each module:

$$P_{total}(t) = P_{screen}(t) + P_{cpu}(t) + P_{net}(t) + P_{GPS}(t) + P_{back}(t) \tag{1}$$

Where each term corresponds to the instantaneous power consumption of different functional modules at time t. The main purpose of this decomposition is to break the system-level energy consumption problem into several relatively independent but still modelable sub-processes, allowing subsequent continuous-time analysis to be carried out in a unified input space.

(1) Screen Power Consumption Model

The screen is one of the relatively stable energy-consuming modules in mobile devices. Its power consumption mainly consists of a baseline display power and a brightness-dependent dynamic component. In practical usage, this part depends not only on whether the screen is on, but also on brightness adjustment.

Therefore, a baseline screen power $P_{screen0}$ and a brightness coefficient k_{screen} are introduced. A screen state variable $s(t) \in [0,1]$ and a normalized brightness $b(t) \in [0,1]$ are defined, leading to:

$$P_{screen}(t) = s(t)\cdot[P_{screen0} + k_{screen}\cdot b(t)] \quad (2)$$

This formulation captures the continuous variation of screen power consumption caused by state switching and brightness changes with relatively low complexity.

(2) CPU Power Consumption Model

CPU power consumption is strongly related to system workload. Even without explicit user interaction, system scheduling and background services still maintain a certain level of baseline power usage. Therefore, CPU power consumption can generally be decomposed into a static component and a load-driven dynamic component [3].

Let the CPU static power be P_{cpu0}, the maximum load power be P_{cpu_max}, and the CPU utilization be $r_{cpu}(t)$, then:

$$P_{cpu}(t) = P_{cpu0} + (P_{cpu_max} - P_{cpu0})\cdot r_{cpu}(t) \quad (3)$$

This model describes the overall trend of CPU power consumption increasing with load and gradually approaching its upper bound, while keeping the structure simple and preserving the key dynamic behavior.

(3) Network Connection Power Consumption Model

The network module includes both Wi-Fi and cellular communication, which share similar power consumption mechanisms. Both involve a connection-maintaining state and a data transmission state. During idle periods, power is mainly used to maintain the connection, while during data transmission, power consumption increases significantly with the data rate.

The Wi-Fi power consumption model is given by:

$$P_{wifi}(t) = w(t)\cdot[P_{wifi_empty} + k_{wifi}\cdot d_{wifi}(t)] \quad (4)$$

Where $w(t)\in[0,1]$ represents the Wi-Fi connection state, and $d_{wifi}(t)$ represents the data transmission rate.

Similarly, the cellular network power consumption is:

$$P_{cell}(t) = c(t)\cdot[P_{cell_empty} + k_{cell}\cdot d_{cell}(t)] \quad (5)$$

Thus, the total network power consumption can be written as:

$$P_{net}(t) = P_{wifi}(t) + P_{cell}(t) \quad (6)$$

This modeling approach captures the joint effect of network connection state and data activity intensity on power consumption, rather than relying on a single factor alone [4].

(4) GPS Power Consumption Model

The GPS module is characterized by a power consumption behavior that is mainly determined by its on/off state. When the location service is disabled, the power consumption is close to zero; once enabled, it maintains a relatively stable level of consumption.

Introducing a state variable $g(t)\in[0,1]$ and an activation power P_{GPS_on}, we have:

$$P_{GPS}(t) = g(t)\cdot P_{GPS_on} \quad (7)$$

This model is relatively straightforward in form, but it effectively captures the on-demand activation nature of GPS energy consumption.

(5) Background Activity Power Consumption Model

Background power consumption has a more complex origin, involving operating system services, application background processes, and low-frequency sensor activities. These behaviors are difficult to model individually, so an equivalent aggregated representation is usually adopted.

Introducing a background activity coefficient k_{back} and a utilization factor $r_{back}(t)$, we obtain:

$$P_{back}(t) = k_{back}\cdot r_{back}(t) \quad (8)$$

This treatment reduces modeling complexity while still reflecting the impact of background processes on overall system energy consumption.

Through the above decomposition, the total smartphone power consumption under continuous time can be expressed as the sum of multiple functional modules. This formulation maintains a clear structure, while each sub-module has explicit physical meaning, enabling subsequent battery state evolution and lifetime prediction models to be driven within a unified input framework.

2.2. Second-Order Thevenin Thermo-Electro Coupled Model

(1) Second-Order Thevenin Electrical Continuous-Time Model

Based on the second-order Thevenin equivalent circuit, a continuous-time state evolution model of the battery can be established [5, 6]. Taking the state of charge (SOC) as the core variable, while also considering battery temperature T and rated capacity Q_n, the SOC dynamics satisfy:

$$\frac{dSOC}{dt} = -\frac{I(t)}{3600Q_n} \quad (9)$$

This relationship is essentially derived from charge conservation, and its physical meaning is straightforward: SOC decreases continuously with discharge current.

In terms of voltage dynamic response, two polarization branches U_1 and U_2 are introduced, corresponding to different time-scale polarization effects. Their state equations are:

$$\frac{dU_1}{dt} = -\frac{1}{R_1(SOC,T)C_1}U_1(t) + \frac{1}{C_1}I(t); \quad \frac{dU_2}{dt} = -\frac{1}{R_2(SOC,T)C_2}U_2(t) + \frac{1}{C_2}I(t) \quad (10)$$

The two branches serve slightly different roles: U_1 mainly captures fast dynamic response, while U_2 represents relatively slower concentration polarization. The purpose of this formulation is not to increase complexity, but to avoid an overly idealized voltage response.

Regarding parameterization, the internal resistance of the battery is generally affected by both SOC and temperature, so an Arrhenius-type formulation is introduced:

$$R_i(SOC,T) = R_i^{ref} \cdot f_{R_i}(SOC) \cdot \exp\left[\frac{E_{a,R_i}}{R_g}\left(\frac{1}{T} - \frac{1}{T_{ref}}\right)\right] \tag{11}$$

Here, $f_{R_i}(SOC)$ describes the nonlinear modulation of resistance by SOC, while the exponential term reflects the effect of temperature on electrochemical reaction rates. This structure is commonly used in battery modeling, but the focus here is to maintain consistent SOC–temperature coupling.

The open-circuit voltage (OCV) is also not constant; it depends on both SOC and temperature. To avoid excessive complexity, a linear temperature correction is adopted:

$$U_{oc}(SOC,T) = U_{oc}^{ref}(SOC) + \alpha_{U_{oc}}(T - T_{ref}) \tag{12}$$

This compromise preserves the SOC-dominant relationship while introducing temperature correction, preventing significant distortion under low- or high-temperature conditions.

According to Kirchhoff's voltage law, the terminal voltage of the battery can be written as:

$$U_L(t) = U_{oc}(SOC,T) - I(t)R_0(SOC,T) - U_1(t) - U_2(t) \tag{13}$$

Considering the power balance relation: $P_{total} = U_L(t) \cdot I(t)$.

Combining these two expressions leads to a quadratic equation in current:

$$I^2 R_0(SOC,T) - [U_{oc}(SOC,T) - U_1 - U_2]I + P_{total} = 0 \tag{14}$$

The corresponding solution for current is:

$$I(t) = \frac{U_{oc} - U_1 - U_2 - \sqrt{(U_{oc} - U_1 - U_2)^2 - 4R_0 P_{total}}}{2R_0} \tag{15}$$

The meaning of this expression is to connect external power consumption with internal electrochemical states, enabling subsequent continuous-time state-space modeling.

(2) Thermo-Electro Coupled Continuous-Time Model

Under high-load conditions, the battery not only experiences electrical losses but also significant thermal effects. Therefore, a heat generation term is introduced:

$$P_{gen} = I^2 R_0 + \frac{U_1^2}{R_1} + \frac{U_2^2}{R_2} + IT\alpha_{U_{oc}} \tag{16}$$

Each term corresponds to ohmic heating, polarization heating, and reversible reaction heat, respectively.

It should be noted that this part is not an additional extension, but rather a supplementary description of energy dissipation pathways.

Based on energy conservation, the temperature evolution equation is:

$$C_{thermal}\frac{dT}{dt} = P_{gen} - h(T - T_a) \tag{17}$$

This equation describes the dynamic balance between heat generation and environmental heat dissipation. In practice, temperature varies more slowly than voltage, but its influence on parameters is persistent.

(3) State-Space Model Construction

Based on the electrical and thermal models, the system can be unified into a state-space representation.

The state vector is defined as: $\mathbf{x} = [SOC, U_1, U_2, T]^T$.

The input vector is defined as: $\mathbf{u} = [P_{screen}, P_{cpu}, P_{net}, P_{GPS}, P_{back}]^T$.

The continuous-time state equation is written as:

$$\frac{d\mathbf{x}}{dt} = f(\mathbf{x}, \mathbf{u}, t) \tag{18}$$

The meaning of this state-space formulation is straightforward: all system dynamics are unified into a continuous-time framework.

This model jointly describes the evolution of electrical and thermal states under continuous time, where power consumption drives SOC variation, which further affects voltage and temperature responses. Compared with a purely electrical model, this coupling better reflects real operating conditions while keeping computational complexity within a manageable range.

2.3. Parameter Estimation and Model Validation

This section performs parameter estimation and validation based on the established power consumption decomposition model and experimental data. It should be noted that the experimental data are mainly used here to verify the consistency between the continuous-time model and actual power consumption behavior, rather than to invert the evolution structure of state variables. Therefore, the role of the data is primarily as a validation tool for model effectiveness, rather than a substitute for modeling.

(1) Parameter Estimation of the Power Consumption Decomposition Model

For the power decomposition model, parameters of each sub-module can be estimated using linear regression. At the system level, assuming an approximately linear relationship between power output and corresponding driving factors, we have:

$$y_i = \alpha_0 + \alpha_1 x_i + \varepsilon_i \tag{19}$$

Where y_i denotes observed power consumption, x_i denotes the corresponding driving factor, and ε_i is the error term.

Parameter estimation is performed using the least squares criterion, with the objective function:

$$\min_{\alpha_0,\alpha_1}\sum_{i=1}^{n}(y_i-(\alpha_0+\alpha_1 x_i))^2 \tag{20}$$

The analytical solution is:

$$\hat{\alpha}1=\frac{\sum i=1^n(x_i-\bar{x})(y_i-\bar{y})}{\sum_{i=1}^{n}(x_i-\bar{x})^2},\quad \hat{\alpha}_0=\bar{y}-\hat{\alpha}_1\bar{x} \tag{21}$$

To evaluate the explanatory power of the model, the coefficient of determination R^2 is introduced:

$$R^2=1-\frac{\sum_{i=1}^{n}(y_i-\hat{y}_i)^2}{\sum i=1^n(y_i-\bar{y})^2} \tag{22}$$

To reflect the stability of parameter estimation, the standard error and confidence interval are also introduced:

$$SE(\hat{\alpha}_1)=\frac{\hat{\sigma}}{\sqrt{\sum(x_i-\bar{x})^2}},\quad SE(\hat{\alpha}_0)=\hat{\sigma}\sqrt{\frac{1}{n}+\frac{\bar{x}^2}{\sum(x_i-\bar{x})^2}} \tag{23}$$

$$\hat{\alpha}_j\pm t_{\beta/2,n-2}\cdot SE(\hat{\alpha}_j) \tag{24}$$

This estimation process imposes statistical significance constraints, ensuring a balance between numerical stability and physical consistency.

The parameters to be estimated in the power decomposition model include $P_{screen0}, k_{screen}, P_{cpu0}, P_{cpu_max}, P_{GPS_on}, P_{wifi_empty}, k_{wifi}, P_{cell_empty}, k_{cell}, k_{back}$.

Figure 1 shows the fitting results of each power consumption sub-module, used to verify the applicability of the decomposition model across different subsystems.

Figure 1(a) corresponds to the relationship between screen power consumption and brightness. The data points are relatively concentrated and exhibit a stable linear trend, with $R^2=0.9431$. The fitting results indicate that the baseline power $P_{screen0}=0.2098W$ and brightness coefficient $k_{screen}=0.6053$ both show good statistical significance, and their confidence intervals do not include zero.

Figure 1(b) corresponds to the CPU power fitting results. The data are more scattered, with $R^2=0.5576$. It can be observed that CPU power consumption is strongly affected by dynamic workload, and the model explains only about half of its variation. The confidence intervals of P_{cpu0} and P_{cpu_max} are relatively wide, indicating strong unmodeled disturbances in CPU power behavior.

Figure 1(c) shows the Wi-Fi power fitting results, which present a relatively stable linear relationship, with $R^2=0.9275$. The estimates of P_{wifi_empty} and k_{wifi} have relatively narrow intervals, indicating high parameter stability under the current data conditions.

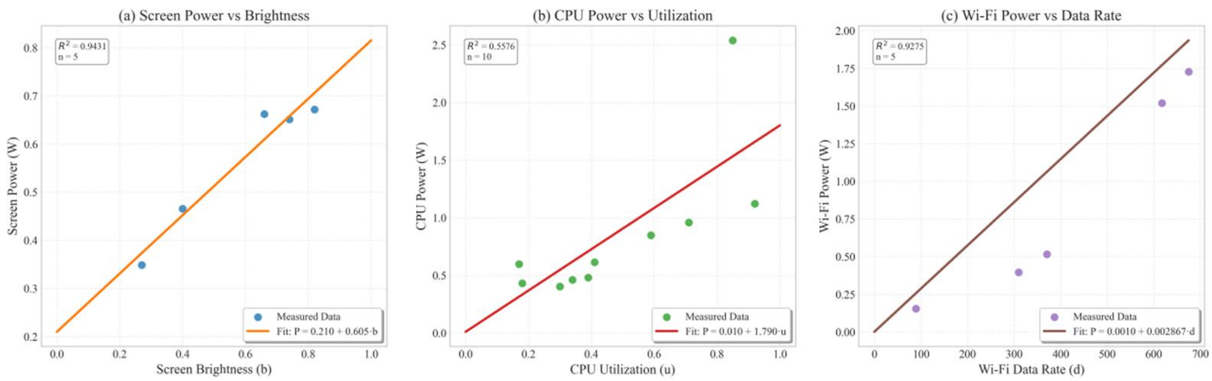

Figure 1. Parameter fitting results of the power model

(2) Parameter Estimation and Validation of the Second-Order Thevenin Model

For the second-order Thevenin thermo-electro coupled model, weighted least squares is used for parameter estimation to balance fitting accuracy among voltage, SOC, and temperature observations.

The objective function is defined as:

$$J(\theta)=J_{U_L}(\theta)+J_{SOC}(\theta)+J_T(\theta)+\lambda|\theta|^2 \tag{25}$$

Where the three error terms correspond to deviations in voltage, SOC, and temperature fitting respectively. The regularization term is used to suppress overfitting and ensure physically reasonable parameter estimates.

The key parameters to be estimated in this model include: $R_0, E_{a,R_0}, \alpha_{U_{oc}}, C_{thermal}, h$.

Figure 2 presents the overall fitting performance of the second-order Thevenin model across multiple physical quantities, used to validate the structural consistency of the model.

The results show that the R^2 values across all subplots range from 0.86 to 0.925, indicating generally low fitting error. Data points are mainly distributed around the fitted curves without systematic deviation, suggesting that the model can stably capture the coupling relationship between electrochemical and thermal dynamics.

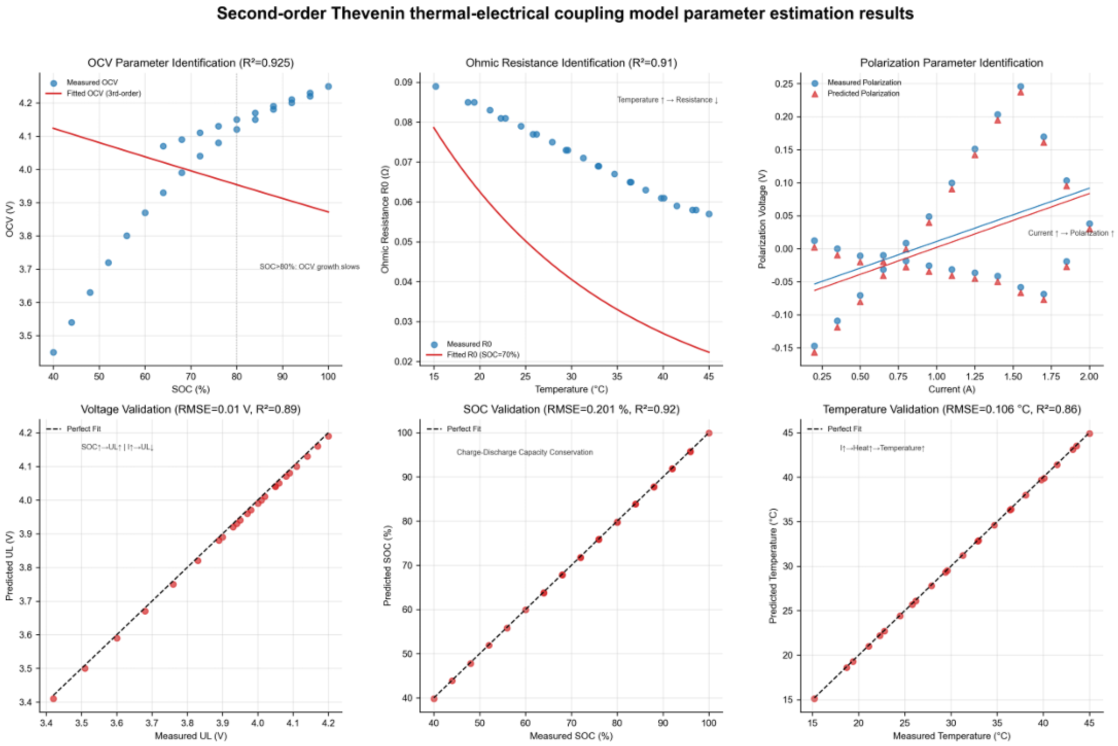

Figure 2. Thermo-electro coupled model parameter validation

In terms of variable coverage, the figure includes multiple dimensions such as OCV, resistance variation, polarization voltage, terminal voltage, SOC, and temperature. Therefore, it not only serves for parameter validation but also reflects the overall consistency of the model structure to some extent.

3. Remaining Discharge Time Prediction via SOC Continuous Decay Dynamics

3.1. Discharge Time Prediction Method

The core problem of battery discharge time prediction is to estimate the time required for the battery to be fully depleted from the current moment, given the current battery state and external load power consumption. This problem essentially describes the continuous decay process of SOC over time, and therefore can be modeled within a continuous-time framework.

From the definition, the discharge time (TTE) can be expressed as the accumulated time corresponding to SOC decreasing from its initial value to zero:

$$TTE = \int_{SOC_0}^{0} \frac{1}{\left|\frac{dSOC}{dt}\right|} dSOC \tag{26}$$

Where SOC_0 represents the initial state of charge, and $\frac{dSOC}{dt}$ denotes the instantaneous rate of SOC change.

The rate of SOC change is determined by both external power input and internal battery parameters, and can be written as:

$$\frac{dSOC}{dt} = -\frac{P_{total}}{U_{oc} \cdot Q_n} \cdot \frac{100}{3600} \tag{27}$$

This relationship indicates that, under a fixed battery capacity, the SOC decay rate is mainly governed by the instantaneous power level, while the open-circuit voltage acts as an energy conversion scale. In other words, higher power consumption leads to faster SOC depletion, a trend that remains relatively stable in practice.

Based on the above model, discharge time under different initial SOC conditions can be further computed. Table 1 shows the comparison between predicted and observed values under the same medium-load condition.

Table 1. Comparison of Remaining Discharge Time under Different Initial SOC Conditions

ID	Initial SOC (%)	Predicted TTE (h)	Actual Value (h)	Deviation (%)
1	100	7.21	6.8–7.5	-1.2 ~ +7.2
2	80	6.27	5.9–6.4	-4.7 ~ +3.2
3	60	4.73	4.5–4.9	-5.0 ~ +5.1
4	40	3.21	3.0–3.3	-4.8 ~ +5.0
5	20	1.67	1.5–1.7	-5.3 ~ +5.3

From the results, under medium-load conditions, TTE shows an approximately linear relationship with the initial SOC, which is consistent with the SOC decay behavior under stable load conditions. Meanwhile, as the initial SOC decreases, the overall discharge time decreases accordingly, which aligns with actual battery behavior.

It should be noted that in the low-SOC region, the prediction error increases slightly. This is mainly caused by the nonlinear voltage drop at low energy levels, which is only approximately treated in the current model through averaging, leading to certain deviations.

Overall, the model can stably capture the trend of discharge time variation across most SOC ranges.

3.2. Uncertainty Quantification and Evaluation

In practical applications, prediction errors arise from multiple sources, mainly including power fluctuation, temperature variation, OCV nonlinearity, and battery self-discharge. These factors jointly form the uncertainty structure of TTE prediction.

The corresponding uncertainty sources and their quantified effects are shown in Table 2.

Table 2. Model Uncertainty Analysis

Source	Impact Level	Quantified Value
Power fluctuation	Dominant	±5%
Temperature variation	Secondary	±3%
OCV nonlinearity	Secondary	±4%

Under the assumption of independent error propagation, the total uncertainty can be approximated as $\sigma_{total} = \sqrt{5^2 + 3^2 + 4^2 + 1^2} = 7.1\%$.

This result indicates that among all error sources, power fluctuation has the most significant impact on prediction performance and plays a dominant role, while self-discharge has a relatively minor effect on the considered time scale.

From a structural perspective, this error distribution suggests that the main source of uncertainty comes from input-side disturbances rather than systematic model bias. Therefore, future improvements can focus primarily on improving power estimation accuracy and enhancing thermal coupling modeling to further improve overall prediction stability.

4. Sensitivity and Stability Analysis via Parameter Perturbation Propagation

Sensitivity analysis is used to characterize how strongly model outputs respond to perturbations in input parameters, thereby evaluating system stability and reliability under parameter variations. In power consumption modeling and battery-coupled systems, this method is not only used to identify key influencing factors but also to observe model behavior under perturbations.

Compared with deterministic calculations, sensitivity analysis further reveals the propagation paths through which parameter variations affect power consumption and voltage outputs. Therefore, it is necessary in complex system modeling.

(1) Uncertainty Propagation Analysis

Under stochastic parameter perturbations, uncertainty propagation analysis of the model output is performed, and the results are shown in Figure 3.

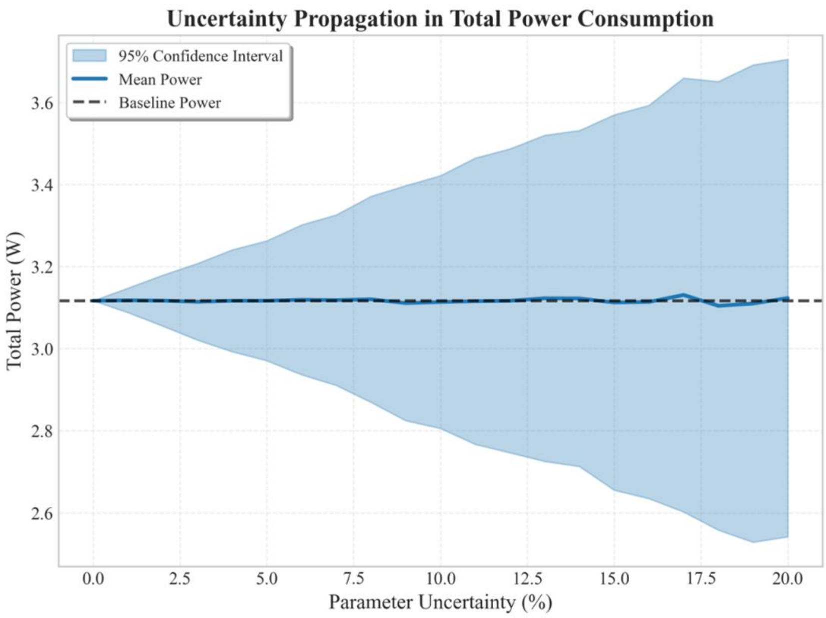

Figure 3. Uncertainty propagation results

Figure 3 shows the distribution of total power consumption when random perturbations within the range of 0%–20% are applied simultaneously to all parameters. It can be observed that as the perturbation magnitude increases, the output distribution gradually spreads, and the confidence interval becomes wider, indicating that errors accumulate within the system.

Under the 20% perturbation condition, total power consumption is mainly distributed between 2.6W and 3.7W, while the mean remains around 3.1168W, with no significant overall shift. From this perspective, the model does not exhibit noticeable drift under parameter perturbations.

In terms of distribution shape, total power consumption remains concentrated within a relatively narrow range, without multimodal behavior or abnormal dispersion. This suggests that the model has a certain degree of statistical stability.

(2) Sensitivity Analysis and Parameter Influence Characteristics

In the second-order Thevenin thermo-electro coupled model, different parameters exhibit significantly different levels of influence on output variables such as terminal voltage. Through comparative analysis of key parameters, the dominant driving factors within the system can be identified.

Overall, parameter influence is not uniformly distributed but instead shows a hierarchical structure. Parameters related to electrochemical reaction kinetics and polarization processes are more sensitive, while thermal-related parameters have relatively weaker effects.

For example, small variations in parameters p_0 and

E_{a,R_0} can cause noticeable fluctuations in the output, indicating that they play a dominant role in the dynamic response of the model. In contrast, parameters such as $C_{thermal}$ have a smaller impact on transient outputs, and even under relatively large perturbations, the resulting output variations remain limited.

It should be noted that this difference is not accidental but is driven by the distinct time scales of electrochemical and thermal processes.

Combining uncertainty propagation and sensitivity analysis results, it can be observed that model output responses to parameter perturbations are mainly concentrated in electrochemical and power-consumption-related variables, while thermal parameters have relatively weaker influence. Under simultaneous multi-parameter perturbations, the model output remains within a stable range without structural deviation, indicating that the model has good robustness within a continuous-time framework.

5. Conclusions

This paper constructs a battery life prediction model based on multi-module power consumption modeling and thermoelectric state coupling, enabling continuous analysis from device operating status to remaining discharge time. Experimental results show that the fit indices for the screen and Wi-Fi power consumption models reached 0.9431 and 0.9275, respectively; the fit results for the second-order Thevenin thermoelectric coupling model ranged from 0.86 to 0.925, indicating that this method effectively reflects changes in battery state. Under different initial SOC conditions, the discharge time prediction error was generally small, with an uncertainty of approximately 7.1%, validating the model's stability and reliability. This study provides a reference for energy consumption prediction and battery management in mobile devices. Future research could further optimize the model's adaptability in complex scenarios.

References

[1] Gong, B. (2021). A study on SOC estimation and remaining life prediction of lithium-ion batteries [Master's thesis]. Anhui University of Science and Technology. https://doi.org/10.26918/d.cnki.ghngc.2021.000173

[2] Dai, M. J., Zhang, L., & Jiang, X. H. (2021). SOC estimation using Kalman filtering based on the second-order Thevenin model. Journal of Hubei University of Automotive Technology, 35(4), 55-58.

[3] Zhao, K. L., Jiang, J. H., Deng, J., et al. (2022). A method for parameter identification of lithium-ion battery equivalent circuit models based on the recursive least squares method with a forgetting factor. Electronic Measurement Technology, 45(16), 87-92. https://doi.org/10.19651/j.cnki.emt.2209936

[4] Wang, H. (2025). SOC estimation of lithium-ion batteries based on adaptive double-extended Kalman filtering [Master's thesis]. Shenyang University of Technology. https://doi.org/10.27322/d.cnki.gsgyu.2025.000395

[5] Chen, Y. (2021). A study on state of charge estimation of lithium-ion batteries based on an improved Thevenin model [Master's thesis]. Hebei University of Technology. https://doi.org/10.27105/d.cnki.ghbgu.2021.001493

[6] Qiao, Z. M. (2020). Analysis of thermal characteristics of lithium-ion batteries based on a thermo-electric coupled model. Power Supply Technology, 44(4), 537-540.